

# Curvature in conformal mappings of 2D lattices and foam structure

A. Mughal and D. Weaire<sup>1,\*</sup>

<sup>1</sup>*Université Paris-Est, Laboratoire de Physique des Matériaux Divisés et des Interface,  
UMR CNRS 8108 5 Bd Descartes, 77454 Marne-la-Vallée cedex 2, France*

(Dated: June 21, 2024)

The elegant properties of conformal mappings, when applied to two dimensional (2D) lattices, find interesting applications in 2D foams and other cellular or close packed structures. In particular the 2D honeycomb (whose dual is the triangular lattice) may be transformed into various conformal patterns, which compare approximately to experimentally realisable 2D foams. We review and extend the mathematical analysis of such transformations, with several illustrative examples, and an account is given of the related work in energy minimisation problems. New results are adduced for the local curvature generated by the transformation.

## I. INTRODUCTION

The relationship  $w = f(z)$ , where  $f$  is any analytical function, can be viewed as a mapping which sets up a correspondence between the points of the  $z$  and  $w$  planes. Such mappings are known as conformal mappings. The geometrical operations of inversion, reflection, translation and magnification are all examples of conformal transformations in Euclidean space. Conformal mappings have a number of interesting properties, the most important being isogonality: any two curves that intersect are transformed into curves that intersect at the same angle.

Consider a discrete 2D set of points in the  $z$ -plane generated by two primitive vectors: the resulting structure in the image plane, due to a conformal mapping, is known as a *conformal lattice*. It is therefore a purely geometrical object. A *strictly conformal crystal* is a physical system consisting of particles located on the sites of a conformal lattice. A *conformal crystal* is a physical system, in which the arrangement of particles approximates a conformal lattice [1].

There are numerous examples of conformal crystals occurring both in nature and in the laboratory; despite this the geometric properties of conformal crystals are at present poorly understood. In the present paper we ask: what determines the local curvature in these conformal patterns? We shall begin our analysis by considering the equation for the complex curvature, which was derived by Needham [2] and also by Mancini and Oguey [3] [4]. For a given line in the  $z$ -plane, we shall see that whereas the first derivative of the transforming function relates the direction of a line to its transformed counterpart, the induced curvature involves the second derivative. Here we shall use the equation for the induced curvature to compute the mean and mean square curvature of the conformal lattice

One of the most easily recognised examples of a nat-

urally occurring conformal crystal is the phyllotactic design of a sunflower [5]. Another example is the so called “gravity’s rainbow” structure, which is the name given to the striking arrangement of arches formed by a cluster of magnetised steel balls in an external force field [5]. More recently, conformal lattices have been shown to have a connection with disclinations in 2D crystalline structures [6] [7].

Conformal crystals can be physically realised by sandwiching an ordered, quasi 2D, foam in a Hele-Shaw cell with non-parallel plates, see for example [8]. Yet another method involves the use of ferrofluid foams in magnetic fields [9]. The advantage of these foam-based methods is that a variety of conformal crystals can be realised by tuning the geometry of the experiment. However, the use of foams to approximate conformal lattices involves two complications which have to be taken into account. Firstly, as was shown by Mancini and Oguey (see [3] [4]) the curvature of the soap films *perpendicular* to the glass plates has to be taken into account (in section III we summarise the main results of the work conducted by Mancini and Oguey). Secondly, we compute the higher order corrections in the expression for the complex curvature and show that is only when these terms are small that the foam is a good approximation to a conformal lattice.

The paper is organised as follows. In section II we introduce the complex curvature and give some properties of conformal transformations. The relationship between ordered 2D soap froths and conformal transformations is detailed in section III. In section IV we calculate the mean curvature and the mean square curvature of the conformal lattice when the original lattice in the  $z$ -plane is free of curvature, for a purely 2D system. We illustrate these results with some examples which include the case of complex inversion. In section V we generalise our results and include the case where the original lattice in the  $z$ -plane has a curvature. In section VI we compute the higher order terms in the expression for the complex curvature. In section VII we discuss some further applications for conformal crystals, these include disclinations in 2D crystals and the intelligent design of 2D computational meshes. Finally, we give our conclusion in section

---

\*Department of Physics, Trinity College, Dublin 2, Republic of Ireland

VIII.

## II. SOME PROPERTIES OF CONFORMAL TRANSFORMATIONS

### A. Scaling of Areas

Although a conformal mapping  $w = f(z)$  preserves angles (the isogonal property) it does not preserve areas. If  $ds_z = (dx^2 + dy^2)^{\frac{1}{2}}$  is a small element of line in the  $(x,y)$  plane, upon being mapped to the  $w$ -plane it will be magnified and have a length given by,

$$ds_w = \left| \frac{dw}{dz} \right| ds_z = |f_1(z)| ds_z, \quad (1)$$

where  $f_n(z)$  is the  $n$ th derivative of the function  $f(z)$ . Hence a small element of area in the  $z$  plane, denoted by  $dA_z$ , will upon being mapped to the  $w$ -plane have an area

$$dA_w = \left| \frac{dw}{dz} \right|^2 dA_z = |f_1(z)|^2 dA_z. \quad (2)$$

### B. Complex Curvature

Consider a curve  $K$  in the  $z$ -plane: if we apply an analytical mapping  $f$  to this curve then it will transform into another curve in the image plane, which we denote by  $\tilde{K}$ .

Let us now choose some arbitrary point on  $K$  which we denote by  $p = x + iy = re^{i\theta}$ . The unit tangent vector to the curve at point  $p$  is given by  $\widehat{\xi}(\phi) = e^{i\phi}$ , where  $\phi$  is the angle the tangent vector makes with the  $x$  axis; for an illustration see the top part of Fig. (1). Upon applying an analytical transformation, point  $p$  is mapped to a new point in the image plane which has coordinates  $f(p) = u + iv = Re^{i\Lambda}$ . It has been shown, see [2], that if the instantaneous curvature of  $K$  at the point  $p$  is given by  $\kappa$ , then the instantaneous curvature at  $f(p)$  is given by,

$$\tilde{\kappa} = \frac{1}{|f_1(p)|} \text{Im} \left[ \frac{f_2(p)}{f_1(p)} \widehat{\xi}(\phi) \right] + \frac{\kappa}{|f_1(p)|}, \quad (3)$$

where  $\text{Im}$  is the imaginary component, see the bottom part of Fig. (1). The first term in Eq. (3) is the curvature in the image plane if  $K$  is a straight line. If however  $K$  has a curvature  $\kappa$ , then in the image plane this additional curvature is scaled by a factor of  $1/|f_1(p)|$ ; again see [2] for a beautiful derivation of these and other results.

**Example:**  $f(z) = z^\alpha$

The utility of Eq. (3) can be demonstrated by a short example. Consider the mapping,

$$w = f(z) = z^\alpha, \quad (4)$$

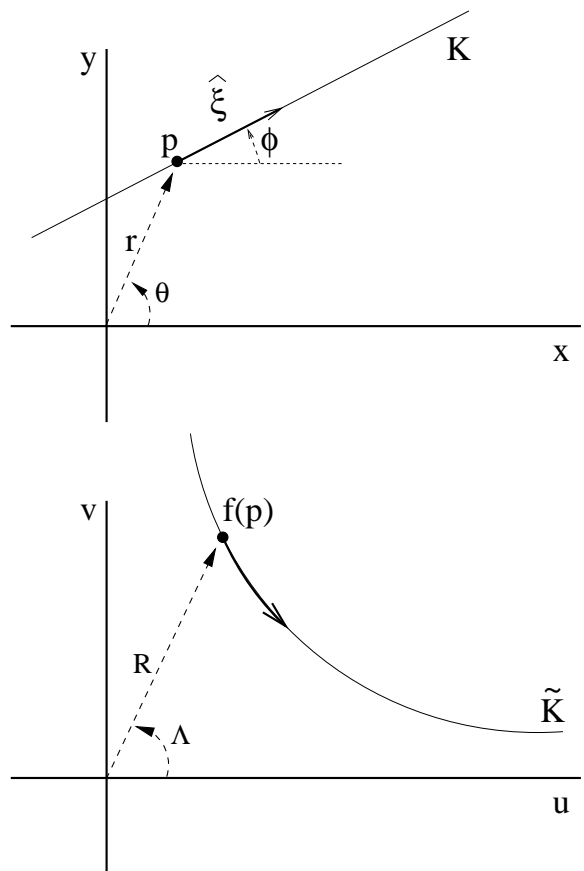


FIG. 1: **Top:** For simplicity we choose to consider a straight line  $K$ , in the  $z$ -plane, which has no curvature (i.e.  $\kappa = 0$ ). As shown the tangent vector  $\widehat{\xi}(\phi)$  at the point  $p$  makes an angle of  $\phi$  with the  $x$  axis. **Bottom:** In the image plane the effect of the analytical mapping is to yield a curve  $\tilde{K}$ , the curvature of which is given by  $\tilde{\kappa}$ . After [2]

where

$$f_1(z) = \alpha z^{\alpha-1} \quad \text{and} \quad f_2(z) = \alpha(\alpha-1)z^{\alpha-2}, \quad (5)$$

and let us represent the  $z$ -plane and the image plane in terms of complex polar coordinates so that,

$$z = re^{i\theta} \quad \text{and} \quad w = Re^{i\Lambda}.$$

Upon substituting Eq. (5) into Eq. (3), we find that the effect of mapping a straight line in the  $z$ -plane (i.e.  $\kappa = 0$ ) is to yield a curve in the  $w$ -plane with curvature,

$$\tilde{\kappa} = \frac{1}{\alpha r^{\alpha-1}} \text{Im} \left[ \frac{\alpha-1}{z} \widehat{\xi}(\phi) \right].$$

Writing out  $\widehat{\xi(\phi)}$  explicitly and simplifying, this becomes,

$$\begin{aligned}\tilde{\kappa} &= \frac{1}{\alpha r^{\alpha-1}} \text{Im} \left[ \frac{\alpha-1}{r e^{i\theta}} (e^{i\phi}) \right] \\ &= \frac{\alpha-1}{\alpha} \frac{1}{r^{\alpha-1}} \text{Im} \left[ \frac{e^{i(\phi-\theta)}}{r} \right] \\ &= \frac{\alpha-1}{\alpha} \frac{1}{r^\alpha} \sin(\phi-\theta).\end{aligned}$$

Note, the curvature is expressed in terms of the coordinates of the  $z$ -plane. To get the curvature in the  $w$ -plane we must use the relationship  $R = r^\alpha$ , which gives

$$\tilde{\kappa} = \frac{\alpha-1}{\alpha} \frac{1}{R} \sin(\phi-\theta).$$

Thus the maximum curvature occurs when the tangent vector is perpendicular to the vector connecting the origin to the point  $p$  and is given by,

$$|\tilde{\kappa}_{max}| = \frac{\alpha-1}{\alpha} \frac{1}{R}. \quad (6)$$

This means that lines, in the  $z$ -plane, drawn perpendicular to the vector connecting the origin with point  $p$  will acquire the greatest curvature, while lines drawn parallel to it will not suffer any curvature.

### III. PROPERTIES OF 2D SOAP FOAMS AND THEIR RELATIONSHIP TO CONFORMAL TRANSFORMATIONS

A dry 2D foam consists of 2D bubbles separated by lines which meet at vertices. Such a foam can be represented by a network consisting of 2D cells separated by 1D edges. Equilibrium conditions impose strict restrictions on the topology and geometry of such a foam network (see [10]): Plateau's law stipulates that the edges can intersect only three at a time and must do so at an angle of  $2\pi/3$ ; the edges themselves have a constant curvature, that is they form circular arcs, and the curvature of the arcs is related to the corresponding pressure difference between the adjacent bubbles by the Laplace-Young relation. As a consequence of the Laplace-Young relation it follows that the sum of the curvatures of the three edges at a given vertex vanishes, or equivalently that the mean curvature of the adjoining edges vanishes.

All of the above conditions are automatically satisfied by complex inversion,  $f(z) = 1/z$ , or more generally a bilinear conformal transformation. A bilinear transformation has the form,

$$f(z) = \frac{az+b}{cz+d}.$$

It can be decomposed into four sequential transformations: translation, inversion, expansion and rotation, and a final translation, for details see [2]. Of these four steps only inversion is not trivial. Conformality ensures that

the mean curvature at each vertex vanishes, while only complex inversion (or a bilinear transformation) has the special property that it will map a circular arc into another circular arc. Given a dry 2D foam structure at equilibrium, inversion will therefore produce a new equilibrium structure; this was discussed by Weaire [10] who used it to provide a neat proof of the Decoration Theorem.

What we refer to as a quasi 2D foam is a foam consisting of a single layer of bubbles trapped between a pair of narrowly separated, parallel, glass plates [11] - such a confining geometry is known as a Hele-Shaw cell. Provided the separation of the glass plates is below a critical value the quasi 2D foam is a good approximation to a 2D foam, i.e. the equilibrium conditions for 2D foams as stated above - Plateau's law and the Laplace-Young relation - also apply to quasi 2D foams to a good approximation. If the separation of the plates is greater than this critical thickness the bubbles undergo a three dimensional instability and the foam is no longer a monolayer [12].

It is important to remember that the boundaries between bubbles in such quasi 2D foams are indeed 2D soap films and not 1D edges as they are often approximated.

In the ideal case, if all the bubbles trapped in the Hele-Shaw cell have the same volume (monodisperse), then an ordered quasi 2D foam can be realised. Upon viewing the Hele-Shaw cell from above (i.e. from the direction perpendicular to the plates) the bubbles are observed to form a honeycomb structure.

Let us now assume that the bottom plate of the Hele-Shaw cell is flat while the upper plate is slightly angled or curved, if the bubbles are monodisperse, then this imposes a specific variation in the area of the bubbles. The variation in the bubble area can be made to closely match the variation required by a given conformal transformation - as stipulated by Eq. (2). Note that although the area of the bubbles (as observed from the direction perpendicular to the bottom plate) may change their volume remains constant, thus the height of the upper surface is related to the analytical function  $f(z)$  by  $h(w) = 1/dA_w$ . This fact has been used to transform the (straight-edged) honeycomb structure, in a variety of ways, to generate approximations of conformal lattices [8] (i.e. conformal crystals), see for example Fig. (2).

However, the use of quasi 2D foams to simulate conformal lattices leads to a contradiction: on the one hand equilibrium conditions demand that the curvature of the soap films is constant; on the other hand only bilinear transformations have the property that the transformed edges have a constant curvature. Thus, with the exception of the bilinear transformation, the resemblance of any quasi 2D foam to its corresponding complex map may be questioned. The resolution to this problem was recently provided by Mancini and Oguey, see [3] [4], by considering the curvature of the soap films perpendicular to the plates of the Hele-Shaw cell.

Here we briefly state the main results derived by

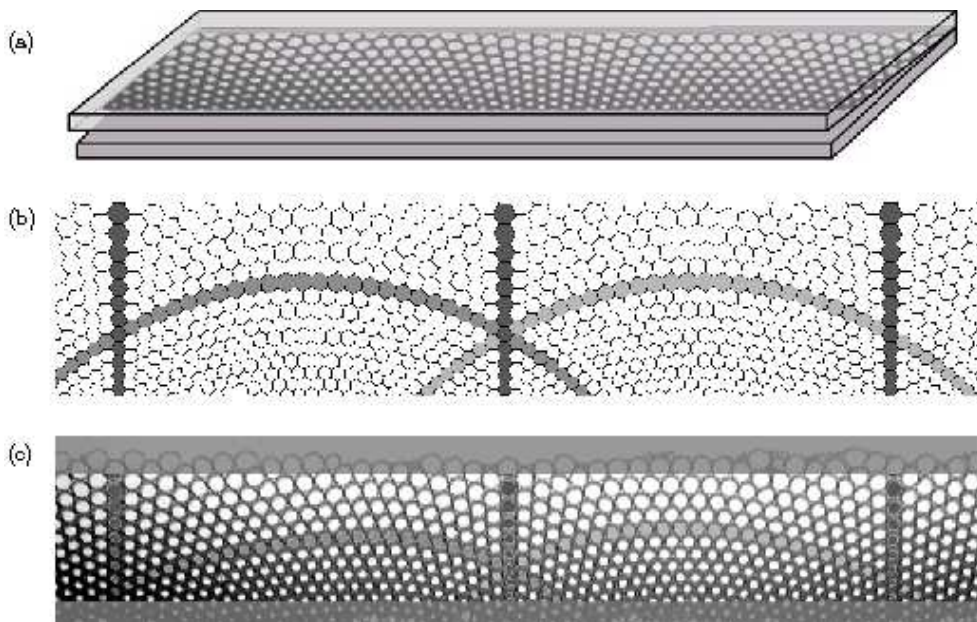


FIG. 2: From [8]: a realisation of the logarithmic map (also known as the gravity's rainbow structure). (a) Experimental setup. Monodisperse bubbles are trapped between two glass plates, the lower plate is horizontal while the upper plate is angled. This arrangement induces specific variation of the bubble area with position in the foam. (b) Numerical mapping of the perfect honeycomb using the transformation  $w = (i\alpha)^{-1} \log(i\alpha z)$ . (c) Experimentally obtained pattern. The shading shows how lines that were initially straight are transformed.

Mancini and Oguey; we refer the reader to their publications for a full account. Fig (3) shows a soap film (dotted line) in a Hele-Shaw cell with non-parallel plates. The height of the top plate, with respect to the bottom plate, is described by a function  $h(x_1, x_2)$ .

The top part of Fig (3) shows the cell from above (i.e. from the direction that is *perpendicular* to the bottom plate). It can be seen that the dotted line, which represents the soap film, has a curvature in the direction parallel to the bottom plate. We shall call this the longitudinal curvature and its instantaneous value at the point  $q$  on the curve is denoted by  $\kappa$ . Fig (3) also shows the normal  $\hat{n}$  and tangent  $\hat{\xi}$  unit vectors to the curve at the point  $q$ .

Now consider the section of the soap film at the point  $q$  as observed from the direction *parallel* to the bottom plate - this is shown in the bottom part Fig (3) - where the upper surface can be assumed to be locally straight by a sufficient magnification close to the point  $q$ . As recognised by Mancini and Oguey if a soap film is sandwiched between two non-parallel plates then, by the normal incidence condition, the film must bend in the direction normal to the plates. We shall call this curvature, which is in the direction perpendicular to the bottom plate, the transverse curvature. By assuming that both  $h$  and  $|\nabla h|$  are small, where  $\nabla h$  locally indicates the direction of maximum slope, to lowest order the transverse curvature

of the soap film is can be shown to be given by

$$\kappa_t \approx -\hat{n} \cdot \frac{\nabla h}{h}$$

Thus Laplace's law can be stated as

$$P_1 - P_2 = 2\gamma H = \gamma(\kappa + \kappa_t) \quad (7)$$

where  $P_1$  and  $P_2$  are the internal pressures of the two bubbles either side of the soap film. Here  $H$  is the total curvature of the soap film.

Mancini and Oguey considered two cases: the first is the trivial case when the pressure is the same for all the bubbles in the conformal crystal (although this case is somewhat artificial from an experimental perspective), the second is where the volume is the same for all bubbles.

For the case of constant pressure it is readily apparent that  $\kappa_t = -\kappa$ , thus the transverse and longitudinal curvatures cancel and  $H = 0$ , this is true for **every soap film** and at **every point** on the soap film.

If on the other hand the volume is constant then it is found that (see [3] and [4])

$$\kappa_t = -2\kappa.$$

The the total curvature, of the soap film, is now not constant but is given by

$$H = \frac{1}{2}(\kappa + \kappa_t) = -\frac{1}{2}\kappa.$$

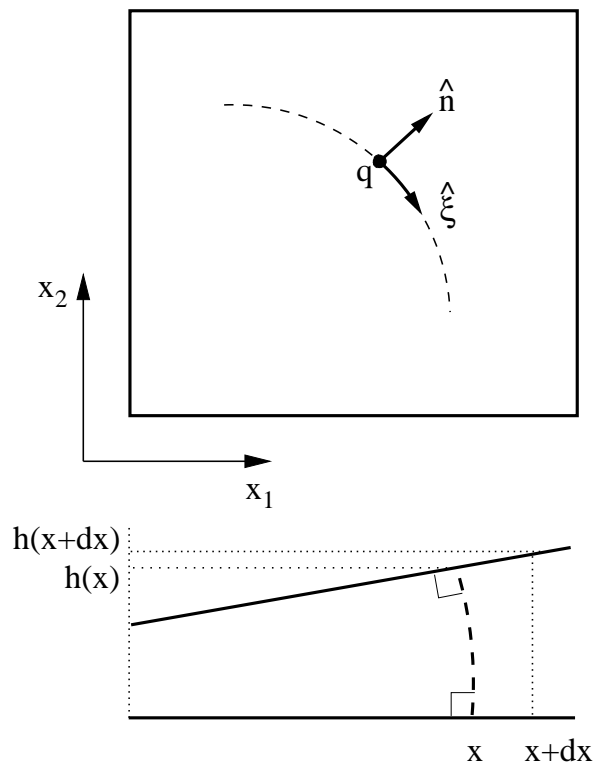


FIG. 3: A soap film (dotted line) confined between a pair of non-parallel glass plates. **Top** This shows the soap film as observed from the direction perpendicular to the bottom plate. For an arbitrary point on the curve, labelled  $q$ , we can define the normal  $\hat{n}$  and tangent  $\hat{\xi}$  unit vectors. The transverse curvature at this point is denoted by  $\kappa$ . **Bottom** After [3] and [4]. This shows the soap film as observed from a direction parallel to the bottom plate. Since the film meets both the top and bottom faces orthogonally it must curve, to lowest order this curvature is given by  $\kappa_t \approx -\hat{n} \cdot \nabla h/h$

This result is remarkable in that for the constant volume case, provided that both  $h$  and  $|\nabla h|$  are small, the total curvature is related in a simple way to the transverse curvature - which can be readily observed in an experimental situation. Again this result holds for **every soap film** and at **every point** on the soap film. Laplace's law, given by Eq. (7), now reads

$$P_1 - P_2 = 2\gamma H = -\gamma\kappa.$$

Since the total curvature is not constant it is important to know by how much the mean curvature deviates from being a constant (as required by the conditions of equilibrium). This discrepancy sets a limit on the applicability of conformal transformations in the context of foams. In section VI we calculate the magnitude of this discrepancy to lowest order.

#### IV. LATTICE CURVATURE AND CONFORMAL TRANSFORMATIONS

For the remainder of this paper we shall only be concerned with complex curvature as defined by Eq. (3). In terms of a quasi 2D soap foam confined in a Hele-Shaw cell with non-parallel plates this is the longitudinal curvature, as defined in the previous section.

In this section we shall examine the curvature that a lattice, in the  $z$ -plane, acquires upon being mapped to the  $w$ -plane. Although the triangular lattice is of primary importance, the results derived are general enough to include other structures. This includes the square lattice and the honeycomb structure.

Consider a vertex in the  $z$ -plane located at  $p=x+iy$ : connected to this vertex there are,  $n = 0, 1, 2, \dots, m \geq 3$ , straight edges. The angular separation between the tangent vectors of successive edges being equal to  $2\pi/m$ . See Fig. (4). In the case of  $n = 6$  or  $n = 4$  it is possible to define two edges, which are connected to the vertex, as primitive vectors and thus tessellate the  $z$ -plane forming triangular or square Bravais lattice, respectively.

We cannot, however, generate the honeycomb structure in the same way (using a vertex with  $n = 3$ ) since the honeycomb structure is not a Bravais lattice. Nevertheless we can tessellate the  $z$ -plane with a honeycomb structure, in a unique way, by making a Voronoi construction of the points which define a triangular lattice. This is because the triangular lattice and the honeycomb structure together define a Voronoi/Delaunay dual, as shown in Fig. (5).

In each case the tessellation in the  $z$ -plane can be thought of as consisting a vertex to which there are connected a number of straight edges of finite length (6 edges for a triangular lattice, 4 edges for a square lattice and 3 edges for a honeycomb structure). In the following we shall examine the effect a conformal mapping has on these edges. We shall compute their curvature in the image plane - from which we can compute the mean and mean square curvature of the edges connected to a given vertex in the image plane.

To keep things simple we only consider the case where the original edges in the  $z$ -plane, connected to a given vertex, are free of curvature. This condition will be relaxed in the next section.

##### A. The Complex Curvature of an Edge Upon Being Mapped to the Image Plane

Upon applying an analytical mapping, the vertex will now be located at a point  $f(p)=u+iv$  in the  $w$ -plane. Since all the edges are straight (i.e.  $\kappa_n = 0$ ), using Eq. (3) it is found that the  $m$  edges have a new curvature

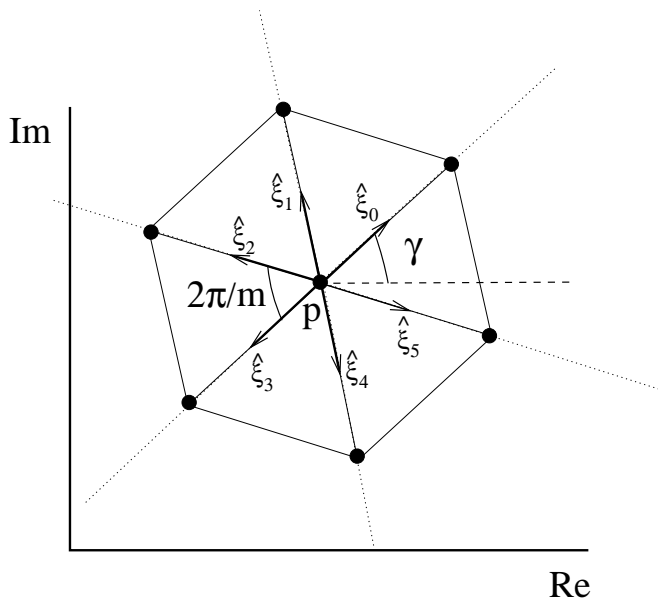


FIG. 4: Consider a vertex located at point  $p$  in the  $z$ -plane, connected to which there are  $m$  straight edges. From the point  $p$  we can draw tangent vectors along each edge which is denoted by  $\widehat{\xi}_0, \widehat{\xi}_1, \dots, \widehat{\xi}_{m-1}$ . The angular separation between the tangent vectors is given by  $2\pi/m$ . We define an angle  $\gamma$  which is the angle between the  $x$ -axis and the first vector  $\widehat{\xi}_0$ . Thus the angle that the  $n$ th vector makes with the  $x$  axis is  $2\pi n/m + \gamma$ . Clearly the edges are invariant under a rotation of  $2\pi/m$  and so we restrict  $\gamma$  to the range  $0 \leq \gamma < 2\pi/m$ .

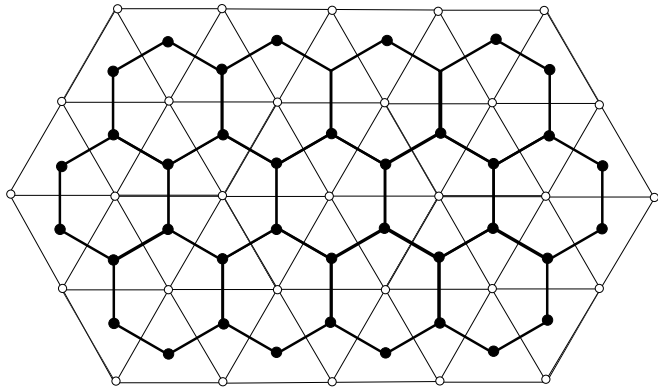


FIG. 5: The white circular points in this diagram represent the lattice sites of a (partial) triangular lattice. The (partial) Voronoi construction partitions the plane into cells each enclosing a single lattice site, where each point inside this cell is closer to that lattice site than to any other. In this diagram the cells generated by the Voronoi construction are drawn using heavy lines, it can be seen that the Voronoi cells form a honeycomb structure. The honeycomb structure can be thought of consisting of a number of vertices (black circular points) to which are connected three edges. Also shown in this diagram is the Delaunay triangulation (drawn using light lines) for the same lattice sites. The Delaunay triangulation is defined as the geometric dual of the Voronoi construction.

given by,

$$\begin{aligned} \widetilde{\kappa}_n &= \frac{1}{|f_1(p)|} \text{Im} \left[ \frac{f_2(p)}{f_1(p)} \widehat{\xi}_n \right], \\ &= \frac{1}{|f_1(p)|} \text{Im} \left[ T e^{i\Theta} \widehat{\xi}_n \right], \\ &= \frac{|f_2(p)|}{|f_1(p)|^2} \text{Im} \left[ e^{i\Theta} \widehat{\xi}_n \right], \end{aligned} \quad (8)$$

where

$$T = \left| \frac{f_2(p)}{f_1(p)} \right|,$$

and

$$\Theta = \theta_2 - \theta_1 = \text{Arg} \left[ \frac{f_2(p)}{f_1(p)} \right],$$

and  $\text{Arg}$  stands for the complex argument. From here on we shall adopt the notation that

$$\theta_n = \text{Arg}[f_n(p)].$$

The  $n$ th tangent vector is given by,

$$\widehat{\xi}_n = e^{i(\frac{2\pi n}{m} + \gamma)},$$

where  $\gamma$  is the angle made by the 0th tangent vector, in the  $z$ -plane, with the  $x$  axis. This is shown schematically in Fig. (4). Eq. (8) can be written as,

$$\begin{aligned} \widetilde{\kappa}_n &= \frac{|f_2(p)|}{|f_1(p)|^2} \sin \left( \Theta + \frac{2\pi n}{m} + \gamma \right), \\ &= \frac{|f_2(p)|}{|f_1(p)|^2} \sin \left( s + \frac{2\pi n}{m} \right), \end{aligned} \quad (9)$$

where  $s = \gamma + \Theta$ .

### B. The Mean Complex Curvature of the Edges, Connected to a Given Vertex, in the Image Plane

Let us define the mean curvature of the edges in the  $z$ -plane as,

$$C_m = \frac{1}{m} \sum_{n=0}^{m-1} \kappa_n,$$

similarly, the mean curvature of the edges in the  $w$ -plane as,

$$\widetilde{C}_m = \frac{1}{m} \sum_{n=0}^{m-1} \widetilde{\kappa}_n. \quad (10)$$

Substituting Eq. (9) into Eq. (10) yields,

$$\widetilde{C}_m = \frac{1}{m} \frac{|f_2(p)|}{|f_1(p)|^2} \sum_{n=0}^{m-1} \sin \left( s + \frac{2\pi n}{m} \right). \quad (11)$$

Using the theorem,

$$\sum_{n=0}^{n=m-1} \sin\left(s + \frac{2\pi n}{m}\right) = 0, \quad (12)$$

it is found that the mean curvature of the edges, connected to a given vertex in the image plane, vanishes. This result is rather trivial it merely expresses the fact that in the image plane, connected to each vertex, there are pairs of opposed edges for which the sum of their curvatures always vanish.

### C. The Mean Square Value of the Complex Curvature of the Edges, Connected to a Given Vertex, in the Image Plane

Since the mean curvature always vanishes, the mean square curvature of the edges in the z-plane is simply defined as,

$$Q_m = \frac{1}{m} \sum_{n=0}^{n=m-1} k_n^2, \quad (13)$$

and in the w-plane the mean square curvature is,

$$\widetilde{Q}_m = \frac{1}{m} \sum_{n=0}^{n=m-1} \widetilde{k}_n^2. \quad (14)$$

Substituting Eq. (9) into Eq. (14) yields,

$$\widetilde{Q}_m = \frac{1}{m} \left( \frac{|f_2(p)|}{|f_1(p)|^2} \right)^2 \sum_{n=0}^{n=m-1} \sin^2\left(s + \frac{2\pi n}{m}\right) \quad (15)$$

Using the theorem,

$$\sum_{n=0}^{n=m-1} \sin^2\left(s + \frac{2\pi n}{m}\right) = \frac{m}{2}, \quad (16)$$

Eq. (15) simplifies to give,

$$\widetilde{Q}_m = \frac{1}{2} \left( \frac{|f_2(p)|}{|f_1(p)|^2} \right)^2. \quad (17)$$

Thus the mean square curvature of the edges, connected to a given vertex in the image plane, is independent with respect to the orientation of the vertex in the image or z planes.

### Examples

To illustrate the results derived for the mean and mean square curvature, we now examine two conformal lattices which have been generated by applying a transformation to a circular disk cut out of a triangular lattice. Just such a cut out is shown in the top left hand part of Fig.(6), it can be seen that the lattice is free of curvature. We examine the case of  $w = z^{1/2}$  and complex inversion  $w = 1/z$ .

*First Example:  $z^{1/2}$*

Applying the mapping,

$$f(z) = z^{1/2}, \quad (18)$$

to the triangular lattice in the z-plane yields a conformal lattice in the image plane, see the top right hand side of Fig.(6). Note, the mapping has been produced by allowing the range of the z-plane to extend to  $\lambda < 4\pi$ .

To find the mean square curvature we substitute Eq. (18) into Eq. (17), which yields

$$\widetilde{Q}_m = \frac{1}{2r} = \frac{1}{2R^2}, \quad (19)$$

where we have transformed from the coordinates in the z-plane  $(r, \lambda)$  to the w-plane coordinates  $(R, \Lambda)$ .

*Second Example:  $1/z$*

Similarly, the effect of inversion is shown in the bottom part of Fig.(6). To compute the mean square curvature substitute

$$f(z) = 1/z.$$

into Eq. (17), which yields,

$$\widetilde{Q}_m = \frac{r^2}{2} = \frac{2}{R^2}. \quad (20)$$

*Comparison with numerical results*

To verify our results we estimate the mean square curvature directly from the transformed lattice. To do so, note that any given hexagonal cell in the image plane can be decomposed into three arcs which cross the the centre of the cell at  $f(p)$ , as shown in Fig. (7). Each of these three arcs can be further decomposed into three points which can be used to fit the equation of a circle, from which the curvature of the arc can be readily computed. Let us denote the three directly computed curvatures as  $\chi_1, \chi_2$  and  $\chi_3$ . We can define the mean square curvature as,

$$|\chi|^2 = \frac{1}{3}(\chi_1^2 + \chi_2^2 + \chi_3^2). \quad (21)$$

Thus, for the two conformal lattices shown in fig 4, we can estimate the mean square curvature for a given vertex using Eq. (21). The results are shown by the black dots in Fig. (8) and Fig. (9), along side are the theoretical results Eq. (19) and Eq. (20).

Except in the case of complex inversion there will be a difference between the analytical value of the curvature and the estimated curvature. This is due to the fact that the curves to which we have fitted the circles are not themselves circular arcs. We quantify this discrepancy in section VI of this paper.

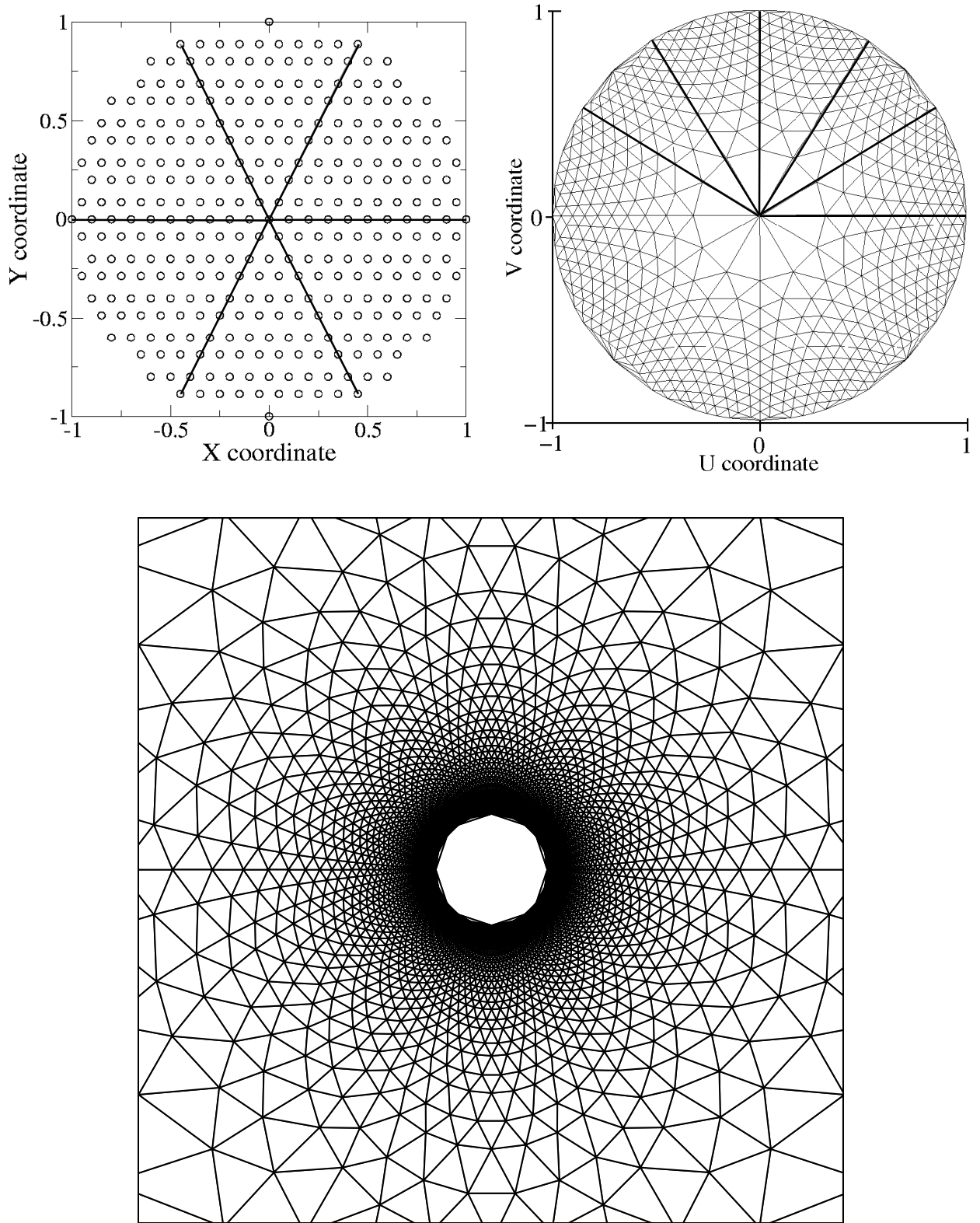


FIG. 6: **Top left:** a circular disk cut out of a triangular lattice in the  $z$  plane, where the angle between each successive heavy line is  $\pi/3$ . Clearly the lattice lines are free of curvature. Upon applying a conformal transformation, **top right:**  $w = z^{1/2}$  and **bottom:** complex inversion, i.e.  $w = 1/z$ , the result is a conformal lattice in the image plane. Note that in the case of  $w = z^{1/2}$  the conformal lattice has been produced by allowing the range of the  $z$  plane to extend to  $\phi < 4\pi$ . In both cases the mean curvature vanishes everywhere but the mean square curvature does not. Also the mean square curvature diverges at the origin, for both transformations the origin is a critical point. At the critical point the angle preserving property of the transformation breaks down, this can be easily seen in the case of the  $w = z^{1/2}$  transformation - instead of being preserved, the angle  $\pi/3$  between rays (heavy lines) emanating from the origin is halved.



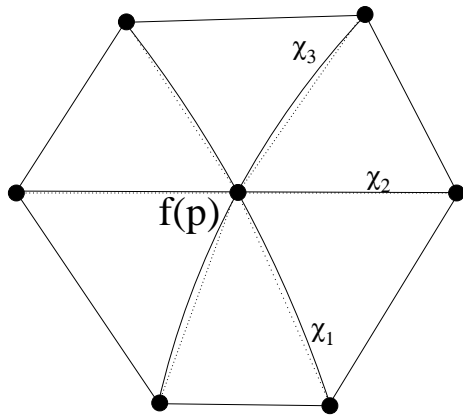


FIG. 7: This diagram shows the effect of the transformation  $f(z)$  on a hexagonal lattice cell, which in the  $z$  plane has its centre at  $p$ . In the  $w$ -plane the lattice cell becomes deformed and its centre is now to be found at  $f(p)$ . The deformed hexagonal cell can be decomposed into three arcs which cross the centre of the cell. Each arc can in turn be decomposed into points, to which we fit the equation of a circle. From this it is possible to calculate the curvature of each arc, represented here by  $\chi_1, \chi_2$  and  $\chi_3$ .

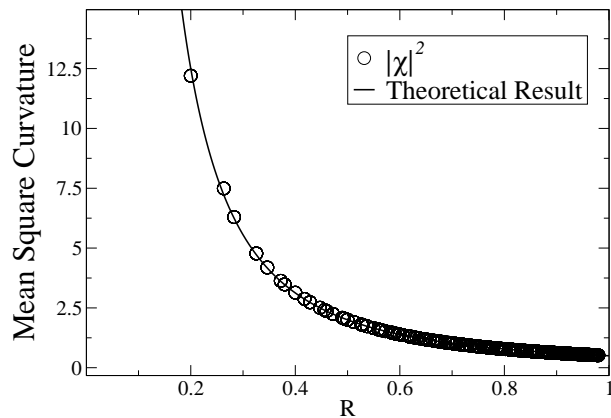


FIG. 8: Mean square curvature for the mapping  $f(z) = z^{1/2}$ : this graph shows a comparison between the theoretical mean square curvature (from Eq. (19)), shown by the continuous line, and the mean square curvature estimated directly from the conformal lattice using Eq. (21), shown by the circles.

## V. SOME GENERALISATIONS

In the previous section we considered a vertex, in the  $z$ -plane, to which there are connected a finite number of straight edges. We found that when the vertex is mapped to the image plane the mean curvature of the edges van-

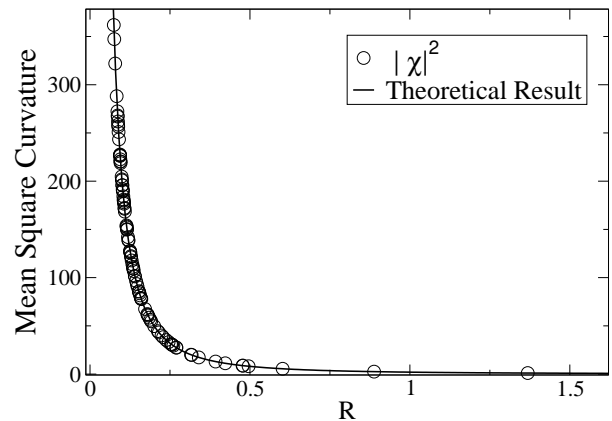


FIG. 9: Mean square curvature for the mapping  $f(z) = 1/z$ : this graph shows a comparison between the theoretical mean square curvature (from Eq. (20)), shown by the continuous line, and the mean square curvature computed directly from the conformal lattice using Eq. (21), shown by the circles.

ishes and that the mean square curvature is independent with respect to the orientation of the vertex.

Let us now consider the case where the edges connected to a vertex, in the  $z$ -plane, have some initial curvature. Let us also assume that the number of edges connected to the vertex is infinite. As the number of edges tends to infinity, the tangent vectors together describe a circle of unit radius centred on the vertex. Upon averaging over the length of the circle the mean curvature of the edges in the  $z$ -plane can be written as,

$$C = \frac{1}{2\pi} \int_0^{2\pi} \kappa(\phi) d\phi, \quad (22)$$

where  $\kappa(\phi)$  is now a continuous function over the range  $0 \leq \phi < 2\pi$  and describes the curvature of the edges in the  $z$ -plane. Similarly, the mean curvature of the edges upon being transformed to the  $w$ -plane is given by,

$$\tilde{C} = \frac{1}{2\pi} \int_0^{2\pi} \widetilde{\kappa(\phi)} d\phi. \quad (23)$$

where we define,

$$\widetilde{\kappa(\phi)} = \frac{1}{|f_1(p)|} \text{Im} \left[ \frac{f_2(p)}{f_1(p)} \widehat{\xi(\phi)} \right] + \frac{\kappa(\phi)}{|f_1(p)|}, \quad (24)$$

Eq. (24) can be written as

$$\begin{aligned} \widetilde{\kappa(\phi)} &= \frac{1}{|f_1(p)|} \text{Im} \left[ T e^{i\Theta} \widehat{\xi(\phi)} \right] + \frac{\kappa(\phi)}{|f_1(p)|}, \\ &= \frac{|f_2(p)|}{|f_1(p)|^2} \text{Im} \left[ e^{i\Theta} \widehat{\xi(\phi)} \right] + \frac{\kappa(\phi)}{|f_1(p)|}, \end{aligned}$$

where  $T$  and  $\Theta$  have the same definitions as in section IV. Writing out  $\xi(\phi)$  explicitly and simplifying gives

$$\widetilde{\kappa}(\phi) = \frac{|f_2(p)|}{|f_1(p)|^2} \sin(\Theta + \phi) + \frac{\kappa(\phi)}{|f_1(p)|}. \quad (25)$$

Substituting Eq. (25) into Eq. (23) yields,

$$\begin{aligned} \widetilde{C} &= \frac{1}{2\pi} \frac{|f_2(p)|}{|f_1(p)|^2} \int_0^{2\pi} \sin(\Theta + \phi) d\phi + \frac{C}{|f_1(p)|} \\ &= \frac{C}{|f_1(p)|}. \end{aligned} \quad (26)$$

Thus the conformal transformation scales the original mean curvature by the magnification factor  $1/|f_1(p)|$  of the transformation (see Eq. (1)).

Since the mean curvature does not necessarily vanish, we define the mean square curvature in the  $z$ -plane as,

$$Q = \frac{1}{2\pi} \int_0^{2\pi} (\kappa(\phi) - C)^2 d\phi, \quad (27)$$

similarly we define the mean square curvature in the  $w$ -plane as,

$$\widetilde{Q} = \frac{1}{2\pi} \int_0^{2\pi} (\widetilde{\kappa}(\phi) - \widetilde{C})^2 d\phi. \quad (28)$$

Expanding Eq. (28) yields,

$$\widetilde{Q} = \frac{1}{2\pi} \int_0^{2\pi} \left( \widetilde{\kappa}(\phi)^2 - 2\widetilde{C}\widetilde{\kappa}(\phi) + \widetilde{C}^2 \right) d\phi, \quad (29)$$

substituting Eq. (25) into Eq. (29) and performing the resulting integrals gives,

$$\begin{aligned} \widetilde{Q} &= \frac{1}{2} \left( \frac{|f_2(p)|}{|f_1(p)|^2} \right)^2 + \frac{Q}{|f_1(p)|^2}, \\ &+ \frac{1}{\pi} \frac{|f_2(p)|}{|f_1(p)|^3} \int_0^{2\pi} \kappa(\phi) \sin(\Theta + \phi) d\phi. \end{aligned} \quad (30)$$

The first term is the mean square curvature of the edges in the image plane if the edges in the  $z$ -plane have no curvature. The second term simply states that the original mean square curvature of the edges is scaled by a factor of  $1/|f_1(p)|^2$ . The third term is a coupling between the original curvature of the edges and the transformation  $f(z)$ .

To get a better understanding of the third term let us label it as  $\widetilde{Q}_3$ . It can be written as,

$$\widetilde{Q}_3 = \frac{1}{\pi} \frac{|f_2(p)|}{|f_1(p)|^3} \int_0^{2\pi} \kappa(\phi) (\sin \Theta \cos \phi + \cos \Theta \sin \phi) d\phi. \quad (31)$$

Since  $\kappa(\phi)$  is an arbitrary function which exists over the interval  $0 \leq \phi < 2\pi$ , it is natural to express it in terms of a Fourier series, so that,

$$\kappa(\phi) = \frac{1}{2} a_0 + \sum_{q=1}^{\infty} a_q \cos(q\phi) + b_q \sin(q\phi). \quad (32)$$

Substituting Eq. (32) into Eq. (31) we find,

$$\widetilde{Q}_3 = \frac{|f_2(p)|}{|f_1(p)|^3} (a_1 \sin \Theta + b_1 \cos \Theta), \quad (33)$$

thus the only contribution to the mean square curvature is from the mode  $q = 1$ . The contributions from all other modes cancel out, so that an increase in mean square curvature for a given edge is cancelled out by a decrease in mean square curvature for some other edge. Furthermore Eq. (33) depends on the orientation of the vertex in the  $z$ -plane, through the angle  $\Theta$  which is the argument of the complex function  $f_2(p)/f_1(p)$  and where  $p$  is the position of the vertex in the  $z$ -plane. The turning points (i.e. the location of the maximum and minimum mean square curvature) depend on the values of the co-efficients  $a_1$  and  $b_1$  and are located at  $\Theta = \tan^{-1}(a_1/b_1)$  and  $\Theta = \tan^{-1}(a_1/b_1) + \pi$ .

Thus when the edges in the  $z$ -plane are not free of curvature the effect of the conformal mapping is to scale the mean curvature, while the mean square curvature is found to be no longer independent with respect to orientation of the vertex.

## VI. HIGHER ORDER TERMS IN THE COMPLEX CURVATURE

In this section we shall distinguish between the instantaneous complex curvature of the image curve, which is given by Eq. (3), and the average complex curvature of the image curve - which we define below.

For a given 2D plane curve its curvature is defined as the rate of change of the angle of the tangent vector with respect to the distance along the curve. We can think of this as limiting process: take two tangent vectors a short distance apart on the curve, measure the angle they make with respect to a fixed axis, and take the limit in which the separation between the tangent vectors vanishes. This then gives the instantaneous value of the curvature. It is in this manner that the expression for the instantaneous complex curvature, given by Eq. (3), is derived.

Consider a 2D plane curve in the image plane which has been generated by applying a complex mapping to some curve in the  $z$  plane. We can choose a pair of points on the image curve a *finite* distance apart and for both points construct a tangent vector. Thus we can ask: what is the rule which gives the total difference in angle between the two tangent vectors?

In this section we derive an expression for the *average* complex curvature which we define as: the total change in the angle of the tangent vector over a segment of a curve averaged over the length of the segment. The result is a series expansion in which Eq. (3) is the lowest order term. This series expansion will lead us to an expression which can be used to measure the degree to which a given image arc differs from being perfectly circular.

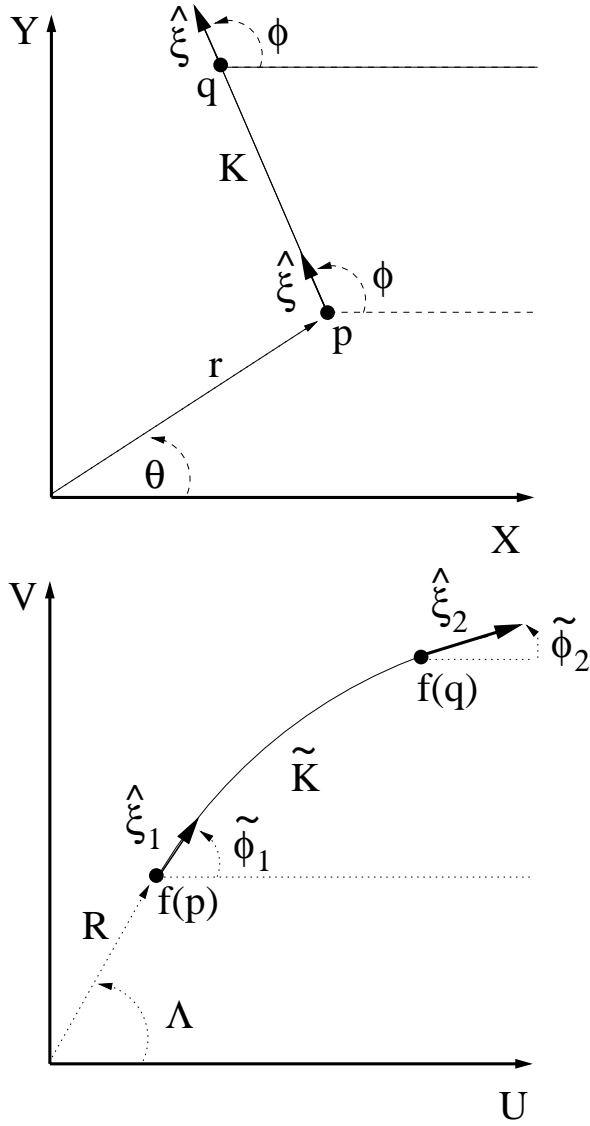


FIG. 10: **Top:** This diagram shows a straight line  $K$  in the  $z$ -plane. The line starts at the point labelled  $p$  and ends at  $q$ , it has a total length  $L$ . At both points the unit tangent vector has the same direction and makes an angle of  $\phi$  with the  $x$ -axis. **Bottom:** This diagram shows the resulting curve  $\tilde{K}$  in the image plane due to the conformal mapping  $w = f(z)$ . The curve begins at the point labelled  $f(p)$  and ends at  $f(q)$  and now has a length  $\tilde{l}$ . In general the angle that the tangent vectors make at  $f(p)$  and  $f(q)$ , which are labelled  $\tilde{\phi}_1$  and  $\tilde{\phi}_2$  respectively, will no longer be equal.

This is an important consideration for the applicability of conformal transformations in the context of foams.

Here we shall only consider the effect of the mapping  $w = f(z)$  on a straight line in the  $z$ -plane. Furthermore, we shall assume that the effect of the mapping is to produce an open, simple and well behaved curve in the image plane.

Consider a straight line  $K$  in the  $z$  plane, which joins

point  $p$  to  $q$  and let us assume it has a length  $|\xi|$ . This is shown in the top part of Fig. (10). At  $p$  we have drawn the unit tangent vector  $\hat{\xi} = e^{i\phi}$ , so that the vector joining  $p$  to  $q$  is given by

$$\xi = |\xi|\widehat{\xi(\phi)}. \quad (34)$$

The line  $K$  is described by the equation

$$K = z(t) = p + t\hat{\xi} = re^{i\theta} + te^{i\phi}, \quad (35)$$

where  $0 \leq t \leq |\xi|$ . Note that at  $t = 0$  we have  $z = p$  and at  $t = |\xi|$  we have

$$z(|\xi|) = q = p + \xi = re^{i\theta} + |\xi|e^{i\phi}.$$

Thus  $K$  has been parametrised by the free parameter  $t$  which measures the distance along  $K$  from the point  $p$ . The line  $K$  has a real component

$$x(t) = r \cos \theta + t \cos \phi,$$

and an imaginary component

$$y(t) = r \sin \theta + t \sin \phi.$$

We notice that since  $K$  is a straight line then the tangent vector is the same at both points  $p$  and  $q$ .

Now consider what happens if we apply an analytical mapping  $w = f(z)$  to  $K$ , the result is a new curve  $\tilde{K}$  in the image plane which starts at the point labelled  $f(p)$  and ends at  $f(q)$  - as shown in the bottom part of Fig. (10). This curve now has some new length which we call  $\tilde{l}$  (not to be confused with the chord distance between  $f(p)$  and  $f(q)$ ).

We define the *average* complex curvature of the image curve  $\tilde{K}$  as

$$\tilde{\mathbb{K}} = \frac{\Delta\tilde{\phi}}{\tilde{l}} = \frac{\tilde{\phi}_2 - \tilde{\phi}_1}{\tilde{l}}. \quad (36)$$

where the tangent vectors at  $f(p)$  and  $f(q)$  are labelled  $\hat{\xi}_1$  and  $\hat{\xi}_2$  and make an angle of  $\tilde{\phi}_1$  and  $\tilde{\phi}_2$ , respectively, with the  $u$  axis.

If for Eq. (36) we keep the point  $p$  fixed and take the limit in which  $|\xi|$  goes to zero we recover the instantaneous curvature of the curve  $\tilde{K}$  at the point  $f(p)$ , that is

$$\tilde{\kappa}(p) = \lim_{|\xi| \rightarrow 0} \tilde{\mathbb{K}},$$

(note that  $\tilde{\kappa}(p)$  refers to the instantaneous curvature of the image curve at the point  $f(p)$ , in keeping with the definition of Eq. (3) we refer to the point  $f(p)$  by its corresponding  $z$ -plane coordinate; of course we are free to express  $\tilde{\kappa}(p)$  in terms of the image plane coordinates  $f(p)$  by making a change of variable - as we did for the example given in section II.B).

Let us now define the difference between the instantaneous curvature of the image arc at its starting point and the average curvature of the arc, which we denote as

$$\Delta\tilde{\mathbb{K}} = \tilde{\mathbb{K}} - \tilde{\kappa}(p).$$

We note that if the image arc is a perfect circle then the instantaneous curvature has a constant value at every point on the arc and therefore  $|\Delta\tilde{\mathbb{K}}| = 0$ . This fact can be used to quantify the degree to which the image curve deviates from perfect circularity.

In the context of 2D and quasi 2D foams it is important to know the degree to which a given arc, generated by a conformal mapping, deviates from perfect circularity. Laplace's law requires that the curvature of a soap film is constant, therefore for a 2D soap film a large value of  $|\Delta\tilde{\mathbb{K}}|$  implies a large error in how well the soap film approximates the conformal lattice. The same holds true for quasi 2D foams (in the constant volume regime), except that we have to remember that the total curvature of the soap film, i.e. the sum of longitudinal ( $\kappa = \kappa(p)$ ) and transverse ( $\kappa_t$ ) curvatures, has an instantaneous value of

$$H = -\frac{1}{2}\tilde{\kappa}(p).$$

In either case Laplace's law is satisfied only if the soap film has a constant longitudinal curvature, i.e. it describes a circular arc when viewed from a direction perpendicular to the bottom plate of the Hele-Shaw cell.

In the following we shall decompose the task of finding  $\tilde{\mathbb{K}}$  into two parts: firstly we compute  $l$  and secondly we compute  $\Delta\tilde{\phi}$ .

### A. Arc Length in the Image Plane

As stated above: the real and imaginary components of the line  $\mathbb{K}$  are a function of the free parameter  $t$ . Upon mapping  $\mathbb{K}$  to the image plane, (using the analytical function  $w = f(z)$ ) the result is the image curve  $\tilde{\mathbb{K}}$  - the real and imaginary components of which are also functions of the free parameter  $t$  and denoted by  $u(t)$  and  $v(t)$ , respectively. We can write the real and imaginary components of  $\tilde{\mathbb{K}}$  in the form of a series expansion about the point  $p$  (i.e.  $t = 0$ ), giving

$$u(t) = u + t\frac{u_t}{1!} + t^2\frac{u_{tt}}{2!} + \dots + \text{h.o.t.} \quad (37)$$

and also

$$v(t) = v + t\frac{v_t}{1!} + t^2\frac{v_{tt}}{2!} + \dots + \text{h.o.t.} \quad (38)$$

where,

$$u = u(t)|_{t=0} = u(0) \quad (39)$$

$$u_t = \left. \frac{du(t)}{dt} \right|_{t=0} \quad (40)$$

$$u_{tt} = \left. \frac{d^2u(t)}{dt^2} \right|_{t=0} \quad (41)$$

and so on. We also define  $v_t$  and  $v_{tt}$  (and higher order terms) in a similar manner.

The total length of the arc  $\tilde{\mathbb{K}}$  is given by,

$$l = \int_0^{|\xi|} \sqrt{\left(\frac{du(t)}{dt}\right)^2 + \left(\frac{dv(t)}{dt}\right)^2} dt. \quad (42)$$

We can substitute Eq.(37) and Eq.(38) into Eq.(42), then expand the integrand in powers of  $t$ , and integrate each term with respect to  $t$  to give,

$$l = l_0|\xi| + l_1|\xi|^2 + l_2|\xi|^3 \dots + \text{h.o.t.} \quad (43)$$

where we assume that  $|\xi|$  is small enough to guarantee convergence of the series. The coefficients in Eq.(43) are defined as

$$l_0 = \sqrt{u_t^2 + v_t^2} \quad (44)$$

$$l_1 = \frac{1}{2} \frac{u_t u_{tt} + v_t v_{tt}}{\sqrt{u_t^2 + v_t^2}} \quad (45)$$

$$l_2 = \frac{1}{6} \sqrt{u_t^2 + v_t^2} \left[ \frac{u_{tt}^2 + u_t u_{ttt} + v_t v_{ttt} + v_{tt}^2}{\sqrt{u_t^2 + v_t^2}} - \frac{(u_t u_{tt} + v_t v_{tt})^2}{2(u_t^2 + v_t^2)^2} \right]. \quad (46)$$

We notice that the coefficients given by Eq.(44) to Eq.(46) (and higher order terms) are defined with respect to the parameter  $t$ . In order to express the coefficients in terms of the complex number  $z$  we use Eq. (35) from which we have the relationship  $dz/dt = e^{i\phi}$ , this can be rearranged to give,

$$dt = e^{-i\phi} dz. \quad (47)$$

Thus Eq.(39) to Eq.(41) (and higher order derivatives) can be written as

$$\begin{aligned} \left. \frac{d^n u}{dt^n} \right|_{t=0} &= \text{Re} \left[ \left. \frac{d^n w}{dt^n} \right|_{t=0} \right] \\ &= \text{Re} \left[ \left. \frac{d^n w}{(e^{-i\phi} dz)^n} \right|_{z=p} \right] \\ &= \text{Re} \left[ \left. \frac{d^n w}{dz^n} \right|_{z=p} e^{in\phi} \right] \\ &= |f_n(p)| \text{Re} \left[ e^{i(\theta_n + n\phi)} \right] \\ &= |f_n(p)| \cos(\theta_n + n\phi) \end{aligned} \quad (48)$$

where in going from the first line to the second line we have made a change of variable from  $t$  to  $z$  and used the fact that at  $t = 0$  we have  $z = p$ ; also we used

$$\left. \frac{d^n w}{dz^n} \right|_{z=p} = |f_n(z)| e^{i \text{Arg}[f_n(z)]} \Big|_{z=p} = |f_n(p)| e^{i\theta_n}.$$

Similarly for the derivatives  $v_t$  and  $v_{tt}$  (and higher order terms), we have,

$$\left. \frac{d^n v}{dt^n} \right|_{t=0} = |f_n(p)| \sin(\theta_n + n\phi). \quad (49)$$

Finally, the coefficients given by Eq.(44) to Eq.(46) can be expressed in terms of Eq.(48) and Eq.(49) to give

$$l_0 = |f_1(p)| \quad (50)$$

$$l_1 = \frac{|f_1(p)|}{2} \operatorname{Re} \left[ \frac{f_2(p)}{f_1(p)} \widehat{\xi(\phi)} \right] \quad (51)$$

$$l_2 = \frac{|f_1(p)|}{12} \left( \frac{|f_2(p)|^2}{|f_1(p)|^2} - \operatorname{Re} \left[ \left( \frac{f_2(p)}{f_1(p)} \widehat{\xi(\phi)} \right)^2 - 2 \left( \frac{f_3(p)}{f_1(p)} \widehat{\xi(\phi)} \right)^2 \right] \right) \quad (52)$$

Upon substituting Eq.(50), Eq.(51) and Eq.(52) into Eq.(43) we have a series expansion in powers of the  $|\xi|$ . We note that the lowest order term in Eq.(43) is identical to Eq.(1).

### B. Change in the angle of the tangent vector in the image plane

We now compute the difference in angle,  $\Delta\tilde{\phi} = \tilde{\phi}_2 - \tilde{\phi}_1$ , of the tangent vectors in the image plane. This derivation is adapted from the one used by Needham to compute the instantaneous curvature [2]. The difference here is that we endeavour to retain all details which may yield higher order terms in the expression for  $\Delta\tilde{\phi}$ .

Consider again the the straight line K in the z-plane, as shown Fig. (10). Note that the tangent vector at  $p$  upon being mapped by the function  $w = f(z)$  is, after being translated to  $f(p)$ , magnified by a length  $|f_1(p)|$  and rotated by an angle  $\operatorname{Arg}[f_1(p)]$ . Similarly, upon applying the mapping  $w = f(z)$ , the tangent vector at  $q$  is, after being translated to  $f(q)$ , magnified by a length  $|f_1(q)|$  and rotated by an angle  $\operatorname{Arg}[f_1(q)]$ . However, the rotation of the tangent vector at  $f(q)$  will differ very slightly by  $\Delta\tilde{\phi}$  from the rotation suffered by the tangent vector at  $f(p)$ .

To compute the difference in angle between the tangent vectors consider the two points p and q as shown on the left hand side of Fig. (11), upon applying the mapping  $f_1(z)$  the points are now located at  $f_1(p)$  and  $f_1(q)$ , respectively. Where the vector connecting  $f_1(p)$  to  $f_1(q)$  is labelled  $\chi$  and is given by

$$\begin{aligned} \chi &= f_1(q) - f_1(p) \\ &= f_2(p)\xi + \frac{1}{2!}f_3(p)\xi^2 + \frac{1}{3!}f_4(p)\xi^3 \dots + \text{h.o.t} \\ &= f_2(p)\widehat{\xi}|\xi| + \frac{1}{2!}f_3(p)\widehat{\xi}^2|\xi|^2 + \frac{1}{3!}f_4(p)\widehat{\xi}^3|\xi|^3 \\ &\quad + \dots + \text{h.o.t} \end{aligned} \quad (53)$$

where we have made use of Eq.(34).

Note, with reference to the right hand side of Fig. (11), that to transform the vector  $f_1(p)$  into the vector  $f_1(q)$

it is necessary to expand the length of  $f_1(p)$  by some factor and to rotate the vector  $f_1(p)$  by an angle  $\sigma$ . It is this angle  $\sigma$  which is the extra rotation suffered by the tangent vector at  $f(q)$  compared to the rotation of the tangent vector at  $f(p)$ , i.e.

$$\sigma = \Delta\tilde{\phi}.$$

Our task is to compute the angle  $\sigma$  shown on the right hand side of Fig. (11). Note,  $\sigma$  is part of a triangle whose sides are given by the known vectors  $\chi$ ,  $f_1(p)$  and  $f_1(q)$ . To compute  $\sigma$  we rotate the triangle shown on the right hand side of Fig. (11) to the real axis by dividing by  $f_1(p)$  (this is the same trick used by Needham [2]), the result is shown in Fig. (12), this new triangle is geometrically similar to the original triangle shown on the right hand side of Fig. (11). The side along the real axis has a length 1 and in addition the point  $\nu$  is given by the vector

$$\nu = [\chi/f_1(p)]. \quad (54)$$

By a simple application of trigonometry we have

$$\Delta\tilde{\phi} = \sigma = \tan^{-1} \left( \frac{\operatorname{Im}[\nu]}{1 + \operatorname{Re}[\nu]} \right). \quad (55)$$

Upon substituting Eq.(54) into Eq.(55), we can expand Eq.(55) in powers of  $|\xi|$  (we assume that  $|\xi|$  is small enough to allow convergence) to give,

$$\Delta\tilde{\phi} = \sigma = \sigma_0|\xi| + \sigma_1|\xi|^2 + \sigma_2|\xi|^3 \dots + \text{h.o.t.} \quad (56)$$

where we have made use of Eq.(53), we find

$$\sigma_0 = \operatorname{Im} \left[ \frac{f_2(p)}{f_1(p)} \widehat{\xi(\phi)} \right] \quad (57)$$

$$\sigma_1 = \frac{1}{2} \operatorname{Im} \left[ \left( \frac{f_3(p)}{f_1(p)} - \left( \frac{f_2(p)}{f_1(p)} \right)^2 \right) \widehat{\xi(\phi)}^2 \right] \quad (58)$$

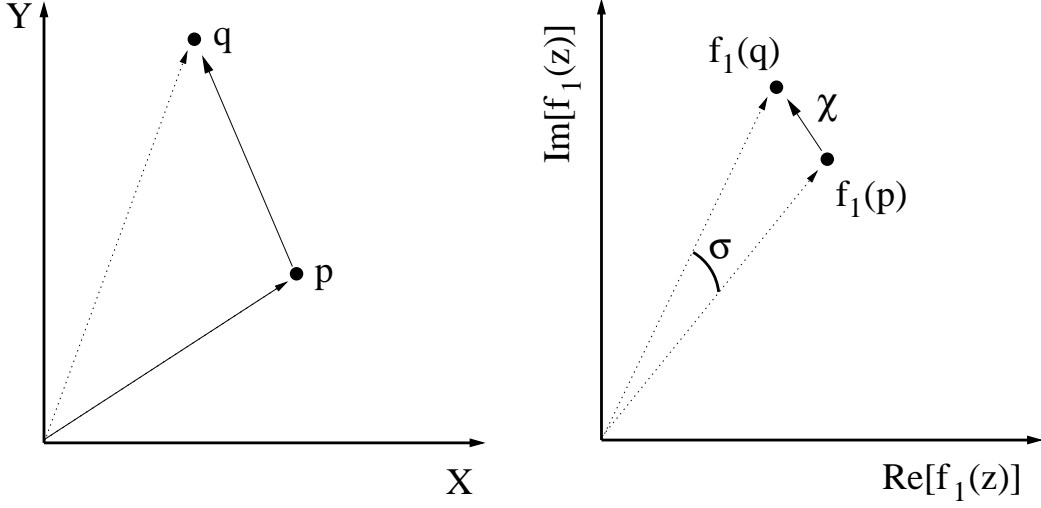


FIG. 11: **Left:** This diagram shows two points  $p$  and  $q$  in the  $z$  plane. **Right:** Upon applying the mapping  $f_1(z) = df(z)/dz$  the points are mapped to  $f_1(p)$  and  $f_1(q)$ , which are connected by the vector  $\chi$ . Note that to transform  $f_1(p)$  into  $f_1(q)$  it is necessary to magnify  $f_1(p)$  by some factor and to rotate  $f_1(p)$  by the angle denoted by  $\sigma$

$$\sigma_2 = \text{Im} \left[ \left( \frac{1}{3} \left( \frac{f_2(p)}{f_1(p)} \right)^3 - \frac{1}{2} \left( \frac{f_2(p)f_3(p)}{(f_1(p))^2} \right) + \frac{1}{6} \left( \frac{f_4(p)}{f_1(p)} \right) \right) \widehat{\xi(\phi)}^3 \right] \quad (59)$$

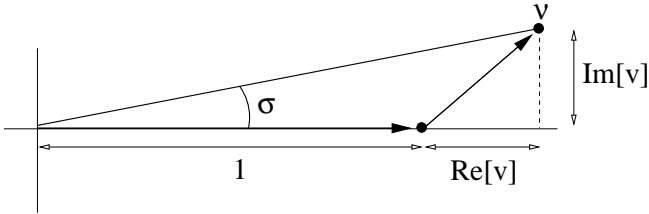


FIG. 12: This triangle is the result of dividing all the vectors shown on the right hand side of Fig. (11) by the complex number  $f_1(p)$ . Dividing by  $f_1(p)$  has two effects: firstly the triangle is rotated so that one of its sides is now parallel to the real axis, secondly all the sides of the triangle are uniformly scaled. This second effect means that the new triangle is similar to the triangle shown in the right hand side of of Fig. (11)

### C. The Average Curvature

Substituting Eq.(43) and Eq.(56) into Eq. (36) and expanding in powers of  $|\xi|$  yields,

$$\widetilde{\mathbb{K}} = \widetilde{\mathbb{K}}_0 + \widetilde{\mathbb{K}}_1|\xi| + \widetilde{\mathbb{K}}_2|\xi|^2 + \dots \text{h.o.t} \quad (60)$$

where we find,

$$\widetilde{\mathbb{K}}_0 = \widetilde{\kappa} = \frac{1}{|f_1(p)|} \text{Im} \left[ \frac{f_2(p)}{f_1(p)} \widehat{\xi(\phi)} \right]$$

$$\begin{aligned} \widetilde{\mathbb{K}}_1 &= \frac{1}{2|f_1(p)|} \left( \text{Im} \left[ \frac{f_3(p)}{f_1(p)} \widehat{\xi(\phi)}^2 \right] \right. \\ &\quad \left. - \frac{3}{2} \text{Im} \left[ \left( \frac{f_2(p)}{f_1(p)} \widehat{\xi(\phi)} \right)^2 \right] \right) \end{aligned}$$

$$\begin{aligned} \widetilde{\mathbb{K}}_2 &= \frac{1}{48|f_1(p)|} \left( \frac{3|f_2(p)|^2}{|f_1(p)|^2} \text{Im} \left[ \frac{f_2(p)}{f_1(p)} \widehat{\xi(\phi)} \right] \right. \\ &\quad + 27 \text{Im} \left[ \left( \frac{f_2(p)}{f_1(p)} \widehat{\xi(\phi)} \right)^3 \right] \\ &\quad - \frac{2|f_2(p)|^2}{|f_1(p)|^2} \text{Im} \left[ \frac{f_3(p)}{f_2(p)} \widehat{\xi(\phi)} \right] \\ &\quad - 34 \text{Im} \left[ \frac{f_2(p)f_3(p)}{(f_1(p))^2} \widehat{\xi(\phi)}^3 \right] \\ &\quad \left. + 8 \text{Im} \left[ \frac{f_4(p)}{f_1(p)} \widehat{\xi(\phi)}^3 \right] \right) \end{aligned}$$

In effect Eq.(60) gives the total change in the angle of the tangent vector in the image plane, as it traverses the image curve, *averaged* over the length of the curve. We observe that as  $|\xi| \rightarrow 0$  then  $\widetilde{\mathbb{K}} \rightarrow \widetilde{\mathbb{K}}_0 = \widetilde{\kappa}$ , giving the instantaneous curvature of the image curve at the point  $f(p)$ . In order to use Eq.(60) we must define the following: (i) a straight line in the  $z$ -plane of length  $|\xi|$ , for which  $\xi = e^{i\theta}$  is the tangent vector at the point  $p = re^{i\theta}$ ; (ii)

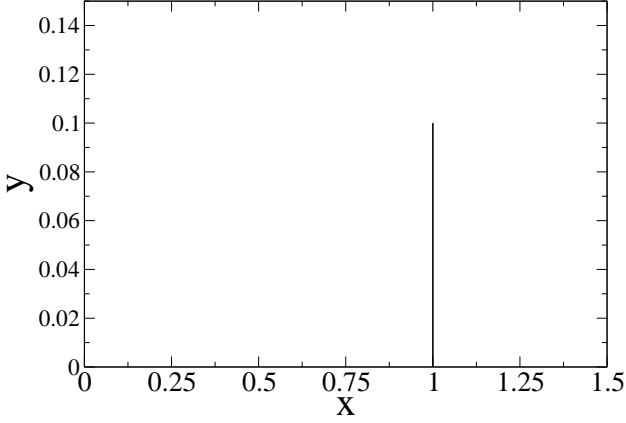


FIG. 13: A straight line in the  $z$ -plane, with  $r = 1, \theta = 0, \phi = \pi/2$  and  $|\xi| = 0.1$

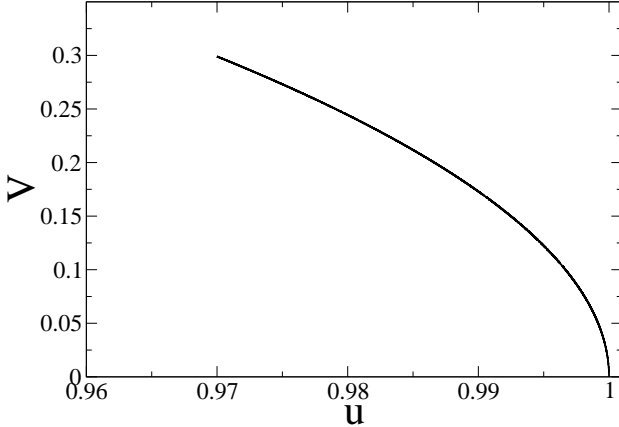


FIG. 14: The resulting curve in the image plane generated by applying the conformal mapping  $f(z) = z^3$  to the straight line defined by Eq.(61)

an analytical function  $f(z)$  which maps the line to the image plane (for which we can compute the derivatives  $f^n(z)$  at the point  $p$ ).

$$\text{Example } f(z) = z^3$$

Let us apply Eq.(60) to two simple examples, we choose the complex mapping  $f(z) = z^3$  and inversion  $f(z) = 1/z$ .

Consider again the a straight line in the  $z$ -plane given

by Eq.(35), and let us set  $r = 1, \theta = 0, \phi = \pi/2$  and  $|\xi| = 0.1$ , so that we have

$$K = z(t) = 1 + te^{i\frac{\pi}{2}}, \quad (61)$$

and  $0 \leq t \leq 0.1$ , the result is the straight line shown in Fig. (13). Upon applying the conformal transformation  $f(z) = z^3$  the result is the curve shown in Fig. (14).

The derivatives for the function  $f(z) = z^3$  are given by  $f_1(z) = 3z^2, f_2(z) = 6z, f_3(z) = 6$ , with all higher derivatives being equal to zero. Upon evaluating these derivatives at the point  $p = re^{i\theta} = 1e^{i0} = 1$  we have  $f_1(p) = 3, f_2(p) = 6$  and  $f_3(p) = 6$ ; together with the angle of the tangent vector to the straight line at the point  $p$  (i.e.  $\phi = \pi/2$ ) and the length of the straight line in  $z$ -plane ( $|\xi| = 0.1$ ), we find

$$\widetilde{\mathbb{K}}_0 = \frac{1}{3} \text{Im} \left[ \frac{6}{3} e^{i\pi/2} \right] = \frac{2}{3} \sin \pi/2 = \frac{2}{3}$$

and similarly  $\widetilde{\mathbb{K}}_1 = 0, \widetilde{\mathbb{K}}_2 = -1/2.25, \widetilde{\mathbb{K}}_3 = 0$  and  $\widetilde{\mathbb{K}}_4 = 0.281481$ ; thus up to fourth order in  $|\xi|$  we have  $\widetilde{\mathbb{K}} \approx 0.66225037$ .

This value can be compared to a numerically computed value. To do so, for the curve shown Fig. (14), we need to compute the length of the curve and the total change in the angle of the tangent vector. This can be done by taking a large number of equally spaced points on the curve. By drawing a straight line between any two adjacent points we get a series of segments which approximate the curve, the approximation improves as more points are taken. It is then a simple matter for a computer to calculate the length of each segment and to find the total length of the curve by summing up the lengths of all the segments. To compute the total change in the angle of the tangent vector: we first compute the angle that the first segment makes with the  $u$  axis, then we compute the angle that the final segment makes with the  $u$  axis, by taking the difference between the two we find the change in the angle of the tangent vector between the start and the end of the curve. Upon taking  $1 \times 10^5$  such equally spaced points on the curve shown in Fig. (14) we have an numerically computed value for the average curvature, giving  $\widetilde{\mathbb{K}}_{\text{Num}} = 0.6622435$ . It is clear that Eq.(60) is converging to  $\widetilde{\mathbb{K}}_{\text{Num}}$  as more terms are taken.

$$\text{Example } f(z) = 1/z$$

Upon carrying out the same procedure outlined above for inversion, i.e.  $f(z) = 1/z$ , also applied to the straight line Eq.(61) (shown in the top part of Fig. (13)), we find  $\widetilde{\mathbb{K}}_0 = \widetilde{\kappa} = 2$  and that all other coefficients  $\widetilde{\mathbb{K}}_1 = \widetilde{\mathbb{K}}_2 = \widetilde{\mathbb{K}}_3 \dots \text{etc} = 0$ . This demonstrates that for a curve produced by complex inversion the instantaneous curvature, at the starting point  $f(p)$  of the curve, is equal to its average curvature. This can only be the case if the curve has a constant curvature and is therefore a circular arc.

### D. Mean Square of the Average Curvature

For the instantaneous curvature we found it useful to compute the mean square curvature. The mean square curvature is independent of the orientation of the vertex and therefore serves as a useful measure of how strongly the conformal lattice is curved at any given point in the image plane.

Similarly we can compute a mean square value of the average curvature. We find that this leads to a series expansion in which the lowest order term is the mean square curvature given by Eq. (17). When the higher order terms in this expansion vanish it means that all the image edges, at that particular point in the image plane, have a constant curvature. If on the other hand the higher order terms do not vanish this means that Laplace's law, for a 2D or quasi 2D foam used to realise the conformal lattice, cannot be perfectly satisfied for every edge. The magnitude of the higher order correction serve as an estimate of the discrepancy between the foam and the conformal map, in most practical cases the discrepancy can be assumed to be negligible if the leading order correction in the expansion is small.

Consider again a vertex  $p$  in the  $z$ -plane to which there are connected a number of straight edges of length  $|\xi|$  separated by a constant angular separation, such as that

shown in Fig. (4). Upon being mapped to the image plane the point  $p$  is now located at  $f(p)$  and the straight edges are transformed into arcs. If we were to sum up the average curvature, for each of the arcs emanating from the vertex at  $f(p)$ , we would find that it vanishes - this is equivalent to saying that the mean of the average curvature always vanishes.

If, however, for each arc we square the average curvature and sum up the squares we have a quantity that does not vanish. Thus we can compute the mean square value of the average curvature  $\widetilde{\mathbb{K}}$ , which we shall denote by  $\widetilde{\mathbb{Q}}$ , this can be done, most easily, by integrating Eq.(60) with respect to  $\phi$  over the range  $0 \leq \phi \leq 2\pi$  giving

$$\begin{aligned} \widetilde{\mathbb{Q}} &= \frac{1}{2\pi} \int_0^{2\pi} \widetilde{\mathbb{K}(\phi)}^2 d\phi. \\ &= \widetilde{\mathbb{Q}}_0 + \widetilde{\mathbb{Q}}_1 |\xi|^2 + O(|\xi|^4) \end{aligned} \quad (62)$$

where we find

$$\widetilde{\mathbb{Q}}_0 = \frac{1}{2} \left( \frac{|f_2(p)|}{|f_1(p)|^2} \right)^2$$

and

$$\widetilde{\mathbb{Q}}_1 = \frac{1}{|f_1(p)|^2} \left( \frac{|f_2(p)|^4}{|f_1(p)|^4} \left( \frac{11}{32} - \frac{5}{12} \operatorname{Re} \left[ \frac{f_1(p)f_3(p)}{(f_2(p))^2} \right] \right) + \frac{1}{8} \frac{|f_3(p)|^2}{|f_1(p)|^2} \right). \quad (63)$$

There are two circumstances under which  $\widetilde{\mathbb{Q}} = \widetilde{\mathbb{Q}}_0 = \widetilde{\mathbb{Q}}$ . The first, which is the trivial case, is when the lattice spacing  $|\xi|$  of the original lattice in the  $z$ -plane vanishes. The second case is complex inversion  $f(z) = 1/z$  (or more generally a bilinear transformation), for which we find  $\widetilde{\mathbb{Q}}_1 = \widetilde{\mathbb{Q}}_2 = \widetilde{\mathbb{Q}}_3 \dots = 0$ . The vanishing of all the higher order corrections means that all the curves emanating from the vertex at  $f(p)$  are circular arcs. It follows that, for a 2D foam or a quasi 2D foam, Laplace's law is satisfied by each of the arcs.

Let us now turn our attention to the mapping  $f(z) = z^{1/2}$  in this case we do not expect Laplace's law to hold for each of the arcs. We have already computed the lowest order term in Eq.(62) and found that

$$\widetilde{\mathbb{Q}}_0 = Q = \frac{1}{2R^2}$$

(see Eq.(19)). Upon substituting  $f(z) = z^{1/2}$  into Eq.(63) we find

$$\widetilde{\mathbb{Q}}_1 = \frac{7}{128} \frac{1}{r^3} = \frac{7}{128} \frac{1}{R^6}.$$

where we have transformed from the coordinates in the  $z$ -plane  $(r, \lambda)$  to the  $w$ -plane coordinates  $(R, \Lambda)$  by using

the relationship  $\sqrt{r} = R$ . Assuming that the original lattice has a constant lattice spacing  $|\xi|$  we can say that a 2D foam, or a quasi 2D foam, is capable of producing a good approximation of a conformal lattice when

$$\widetilde{\mathbb{Q}}_1 |\xi|^2 = \frac{7}{128} \frac{|\xi|^2}{R^6}$$

is small. We see that this happens at regions a large distance from central (critical) point of the conformal lattice, i.e when  $R \gg (7/128)^{1/6} |\xi|^{1/3}$ .

## VII. RELATED WORK

Recently, the subject of conformal lattices with circular symmetry, of the type  $f(z) = z^\alpha$ , such as that shown in the top right hand part of Fig. (6), has been considered from the context of 2D crystals with non-uniform density by Mughal and Moore [6].

The authors performed simulations to find the ground state of a cluster of (classical) electrons confined to move on a disc. As expected, the charge density of the system is non-uniform, being small at the centre of the sys-



tem and very large towards the edge. The positions of the charges in the resulting ground state are triangulated using the Delaunay triangulation package Qhull, this allows the authors to uniquely define the number of nearest neighbours for each charge. The resulting triangulation is then visualised using the package Geomview, see for example Fig. (15) - this image is from [6],

By this method it is found that the ground state is crystalline and that most charges have six nearest neighbours. However, the cluster also contains a large number of defects in its *interior*. These defects are of two types: disclinations and dislocations.

A disclination is any point which has an anomalous coordination number, that is any charge for which the number of nearest neighbours is not equal to six (or four on the cluster edge). A disclination is defined to have a +1 (-1) topological charge if its coordination number is equal to five (seven) - a similar rule applies to charges on the cluster edge. Topological constraints, due to Euler's theorem, ensure that the total topological charge in the system always sums to +6, i.e. there are always 6 more positive disclinations than negative ones.

A dislocation, on the other hand, is defined as a tightly bound pair of disclinations of the opposite charge. Since dislocations are topologically neutral their numbers are not restricted by topology. Instead they are present in the lattice for energetic reasons.

Disclinations induce an enormous elastic stress in the lattice. Consequently, in the ground state of 2D systems which form a triangular lattice with uniform density [13], the 6 positive disclinations demanded by topology are located on the edge of the lattice. In the case of systems with non-uniform density, Mughal and Moore [6] showed that disclinations are found in lattice *interior*. Specifically, a system whose density increases (decreases) upon going from the centre towards the edge must contain more negative (positive) disclinations in its interior than positive (negative) ones. The total disclination charge must still sum to +6. In the case of the system shown in Fig. (15), it is found that for every negative disclination in the system interior there is a compensating positive disclination on the edge of the system. In addition, a further six positive disclinations are located on the edge to satisfy Euler's theorem.

Mughal and Moore demonstrated that these interior disclinations are the mechanism by which the system maintains a crystalline structure while having a non-uniform density. However, the price that the system pays is the loss of translational and rotational symmetries, or in other words, the lattice acquires curvature. Using the framework of Burgers circuits and Burgers vectors, which is the natural way of characterising lattice defects, the authors are able to relate the rate of change of the lattice density to the density of defects. In addition, the authors derive a relationship between the density of defects and the magnitude of the lattice curvature.

During the course of this work the authors were led to consider conformal lattices. They suggested that the cen-

tral point of the transformation of the type  $f(z) = z^\alpha$ , i.e. the critical point, should be considered as a disclination. The parallels between a disclination and the critical point in a conformal transformation of the type  $f(z) = z^\alpha$  are clear: both have an anomalous coordination number, the lattice density is increasing/decreasing upon going away from the critical point/disclination and finally in both cases the surrounding lattice has a curvature.

By treating the critical point, in a conformal lattice of the type  $f(z) = z^\alpha$ , as an isolated disclination at the centre of the cluster, the authors were able to successfully compute the density of the conformal lattice (independently of Eq. (1)) and the magnitude of the lattice curvature. It is satisfying to see that the expression given for the maximum lattice curvature in this earlier work agrees with Eq. (6). Conversely, the same theoretical arguments suggest that the ground state of a cluster containing internal disclinations, such as that shown in Fig. (15), is conformal everywhere *except* at the disclinations.

A recent paper by Rivier et. al. [7] also reaches the same conclusion: a disclination in a 2D crystalline structure can be regarded as a singularity, of the type  $f(z) = z^\alpha$ , in the complex plane. This connection between conformal mapping and topological defects opens up an interesting avenue of research which we shall now discuss.

Considerable effort has been devoted to finding the minimum energy configurations of interacting particles confined to 2D surfaces with a frozen topography. Simulations and experiments have shown that the particles form an ordered triangular structure, in which most particles have six nearest neighbours [14]. In addition the ground state must also contain disclinations (and dislocations). Once again the total disclination charge of the system depends on topology, for example: on a sphere the total disclination charge must sum to +12 while on a torus it is equal to 0 (in these studies the choice of the interaction potential between particles leads to a uniform density of particles on the surface), see [15] and [16]. Such work has shown that even when disclinations are not required by topology, as in the case of the torus [16], they can nonetheless be present in the ground state in response to the Gaussian curvature of the underlying topography.

The consideration of such problems, which are essentially concerned with finding the best way to uniformly arrange particles on an arbitrary surface, finds uses in the generation of computational meshes. The sites at which the particles are located, in the minimum energy configuration, can be used to define a computational mesh for numerically solving partial differential equations. This technique has been used in the computational modelling of a host of physical phenomena, see for example [17] and references therein. Critically, the quality of the mesh for computational purposes depends on factors such as the mesh shape, size and smoothness. However, even for a modest number of particles a great deal of computational effort is required to find the optimal arrangement.

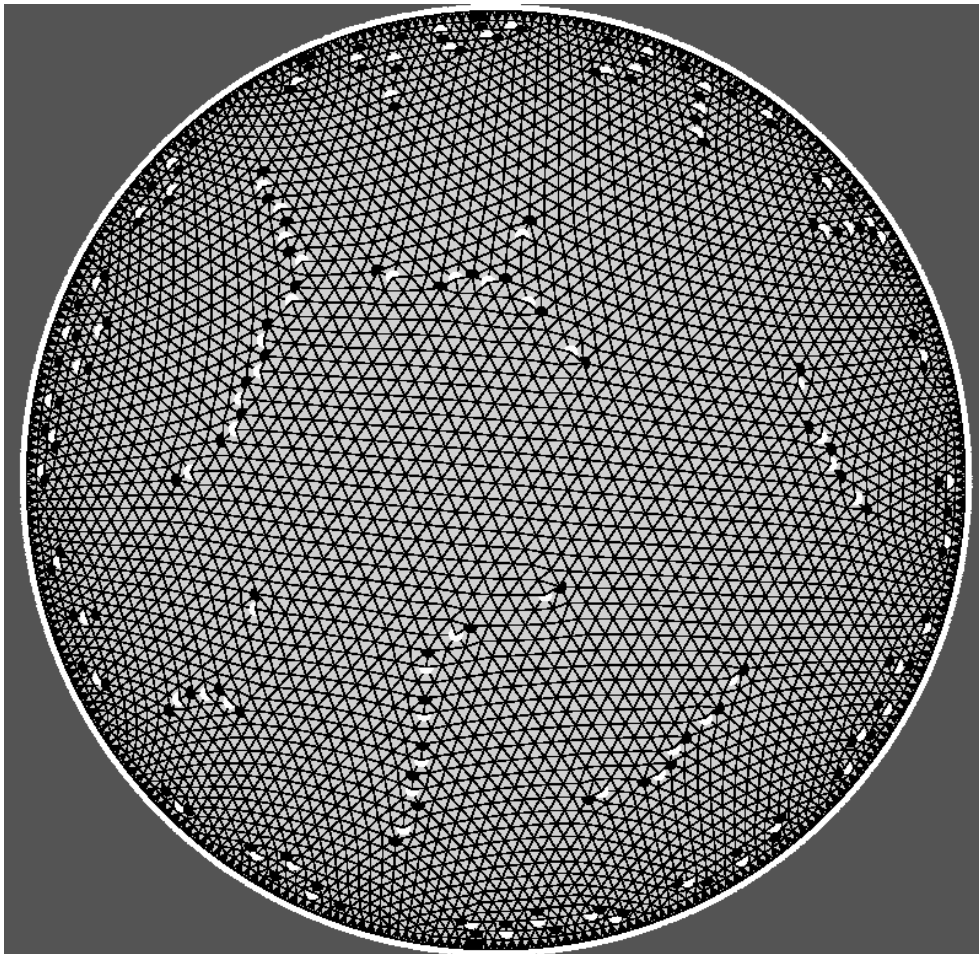


FIG. 15: From [6], with kind permission **5000 (classical) charges in a hard wall confining potential**. The ground state of the system is crystalline with a non-uniform density. The density being smallest at the centre of the system and greatest towards the edge. The cluster interior contains disclinations, these are points whose coordination number is not equal to 6. A disclination has a positive (negative) topological charge if its coordination number is less (greater) than 6. In this image positive (negative) disclinations are coloured white (black). Note, as a consequence of the non-uniform density, the system contains more negative disclinations in its interior than positive ones. This excess of internal disclinations gives rise to the lattice curvature, which can be clearly seen towards the edge of the system.

In response to this, more recent developments have shifted the focus from finding the optimal arrangement of the particles to finding the optimal arrangement of the defects themselves. This approach, pioneered by Bowick et. al. [18], integrates out the underlying triangular lattice to directly make the defects the degrees of freedom. The result is an elastic Hamiltonian, which can be numerically optimised to give the optimal configuration of the defects. This approach has the advantage of reducing the number of degrees of freedom and has been successfully used to find the arrangement of defects on the surface of a sphere [18]. The price that we pay for this decrease in computational burden is that the details describing the underlying lattice are lost.

Knowing the position of the defects in itself is not sufficient information to use this algorithm for generating computational meshes. This is where conformal lattices

might be useful. The idea is that once the optimal number and arrangement of disclinations in the system has been determined using the algorithm outlined in [18], the underlying lattice can be reconstructed by using a series of conformal transformations of an initial regular lattice. This approach may eventually lead to a more intelligent design of computational meshes. This is a topic currently being investigated by the present authors.

### VIII. CONCLUSION

As detailed in [8], the conformal transformation of the honeycomb structure can produce ideal, dry, foam structures that approximate some that can be realised in the laboratory. But the true equilibrium structure is slightly different, in that the local curvature is required to be

constant along each edge. This discrepancy sets limits on the applicability of conformal transformations in the context of foams. The results presented in section VI will be useful to experimentalists working in this field to *estimate* the magnitude of this discrepancy.

Higher order terms for all the expansions given in this paper are available from AM (adil.m.mughal@gmail.com).

## IX. ACKNOWLEDGEMENTS

DW acknowledges support from SFI, ESA and CNRS (visiting position at the group of Prof M Adler, Univ.

Paris-Est). AM would like to thank M. A. Moore and S. Cox for numerous useful discussions. AM and DW are grateful to W. Drenckhan for advice and useful discussions. AM is also grateful to DW and the Foams and Complex Systems group, Trinity College Dublin, for financial assistance for short visits. AM is grateful to S. Cox and the Institute of Mathematical and Physical Sciences, Aberystwyth University, for financial assistance to attend the 2007 winter meeting of the British Society of Rheology.

- 
- [1] F. Rothen and P. Piotr, *Phys. Rev. E* **53**, 2828 (1996).
  - [2] T. Needham, *Visual Complex Analysis* (Oxford University Press, 1997).
  - [3] M. Mancini and C. Oguey, *Colloids and Surfaces A: Physiochem. Eng. Aspects* **263**, 33 (2005).
  - [4] M. Mancini and C. Oguey, *Eur. Phys. J. E* **17**, 119 (2005).
  - [5] F. Rothen, P. Pieranski, N. Rivier, and A. Joyet, *Eur. J. Phys.* **14**, 227 (1993).
  - [6] A. Mughal and M.A. Moore, *cond-mat/0702652* (2007).
  - [7] N. Riviera, M.F. Mirib, and C. Oguey, *Coll. and Surf. A* **263**, 39 (2005).
  - [8] W. Drenckhan, D. Weaire, and S.J. Cox, *Eur. J. Phys.* **25**, 429 (2004).
  - [9] F. Elias, J.C. Bacri, F.H. de Mougins, and T. Spengler, *Philosophical Magazine Letters* **79**, 389 (1999).
  - [10] D. Weaire, *Phil. Mag. Lett.* **79**, 491 (1999).
  - [11] D. Weaire and S. Hutzler, *The Physics of Foams* (Oxford University Press, 2001).
  - [12] S.J. Cox, D. Weaire, and M.F. Vaz, *Eur. Phys. J. E* **7**, 311 (2002).
  - [13] L.J. Campbell and R.M. Ziff, *Phys. Rev. B* **20**, 1886 (1979).
  - [14] A.R. Bausch, M.J. Bowick, A. Cacciuto, A.D. Dinsmore, M.F. Hsu, D.R. Nelson, M.G. Nikolaides, A. Travesset, and D.A. Weitz, *Science* **299**, 1716 (2003).
  - [15] M.J. Bowick, A. Cacciuto, D.R. Nelson, and A. Travesset, *Phys. Rev. B* **73**, 024115 (2006).
  - [16] M.J. Bowick, D.R. Nelson, and A. Travesset, *Phys. Rev. E* **69**, 041102 (2004).
  - [17] P. Knupp, *J. Phys.: Conference Series* **46**, 458 (2006).
  - [18] M.J. Bowick, D.R. Nelson, and A. Travesset, *Phys. Rev. B* **62**, 8738 (2000).